
Property Studies of “Loner” Flares of Gamma-Ray Blazars

Gege Wang^{1,2}, Zhongxiang Wang¹, Liang Chen¹, Jianeng Zhou¹, & Yi Xing¹

¹Shanghai Astronomical Observatory, Chinese Academy of Sciences, Shanghai 200030, China

²Graduate University of the Chinese Academy of Sciences, No. 19A, Yuquan Road, Beijing 100049, China

Received (2019 April 8); Accepted (2019 October 29)

Abstract

We search through γ -ray data obtained with the Large Area Telescope (LAT) onboard the *Fermi Gamma-Ray Space Telescope* and find 24 blazars (or candidates) that have a single clear flare event in their 9.5 year long-term light curves. We define these events as loner flares since each flare stands out significantly above the relatively stable, low-flux light curve. We analyze the LAT data in detail for these 24 sources. The flares in ten of them are primarily due to a single sharp peak, for which we study by fitting with two different analytic functions. The time durations thus determined for the sharp peaks are in a range of 4–25 days. The γ -ray spectra of the 24 blazar sources can be described with a power-law or a log-parabola function. We obtain their spectral properties in the flaring and quiescent states, and find that in the flares 16 of the sources have harder emission and three have softer emission while the other five keep the same emission. We discuss a possible correlation between the differences in photon index in the quiescent and flaring states and photon indices in quiescence. In addition, the sharp peak flares seem to have a tendency of having long time durations and hard emission, possibly related to their physical origin in a blazar jet. Studies of more similar flares will help establish these possible features.

1 Introduction

Since its launch in June 2008, the Large Area Telescope (LAT) on board the *Fermi Gamma-ray Space Telescope* (*Fermi*) has conducted observations at γ -ray energies of 0.1–300 GeV over 10 years by scanning the whole sky every three hours. More than 3000 sources have been reported in the *Fermi* LAT third source catalog (3FGL; Acero et al. 2015), and nearly 5000 sources have been very recently listed in the LAT fourth source catalog (4FGL; The Fermi-LAT collaboration 2019a). From the observations, large amount of data are collected for the detected sources, now allowing detailed analysis for the purpose of studying different properties of the sources.

From *Fermi* LAT, it has been well established that the dominant γ -ray sources in the sky are blazars (Ackermann et al. 2015; The Fermi-LAT collaboration 2019b). These subclass sources of the Active Galactic Nuclei (AGN) have a jet pointing close to the line of sight. Due to the relativistic beaming effect, emission from the jet dominates over that from the host galaxy over nearly the entire electromagnetic spectrum, and thus blazars are characterized by rapid and large-amplitude flux variations (e.g., Ulrich et al. 1997). The all-sky monitoring capability of the *Fermi* LAT has provided us with light curve and spectral data for more than 1800 identified and candidate blazars (Ackermann et al. 2015; and ~ 2800 in the very recently updated fourth catalog of AGN detected with LAT; The Fermi-LAT collaboration 2019b). Many studies have been carried out, while focusing on bright γ -ray blazars and their flares, and related fast variability and spectral changes (some combined with multi-band observations; e.g., Nalewajko 2013; Harris et al. 2014; Kushwaha et al. 2014; Hayashida et al. 2015; Ackermann et al. 2016; Meyer et al. 2019; also for recent reviews of AGN at γ -ray energies, see Dermer & Giebels 2016; Madejski & Sikora 2016). The studies have provided constraints on the physical properties of the jet emission zones and emission processes.

Generally blazars appear to vary randomly, with their power spectral densities (PSDs) often described with a power law (e.g., Chatterjee et al. 2008; Abdo et al. 2010; Chatterjee et al. 2012). The noise-like fluctuations can be explained as due to the presence of many turbulent cells, driven by instability or magnetic reconnection. Sometimes a significantly bright flare may be seen above minor fluctuations for a blazar, and it is intriguing to check the properties of

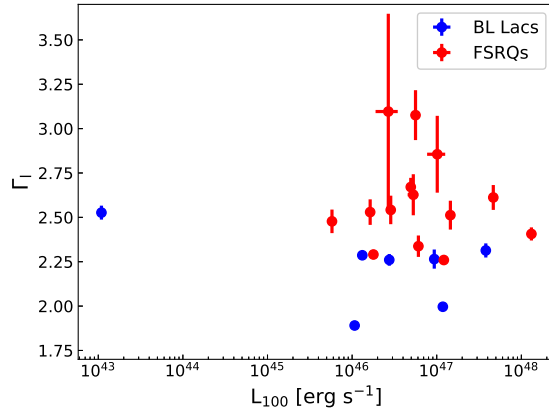


Fig. 1. Photon indices (Γ in a power law or α in a log-parabola) and 0.1–100 GeV luminosities of 21 blazar targets (with redshifts) in the quiescent state.

such flares, how they arise and decay and whether their spectra have significant changes. The properties help understand the underlying physical processes. In our systematic analysis of *Fermi* LAT data for obtaining long-term light curve information for γ -ray blazars, which was based on 3FGL, we have noted one type of “loner” flares. They appeared as one single event lasting comparatively short (most with a time duration of three months) while in most time the blazar source has been in a relatively quiescent state without other strong flaring activity. More specifically, in our 90-day binned light curve data, one to three data points stand out significantly as a flare above the otherwise low-flux flat light curve. We have selected these loner flare sources as our targets, for the purpose of studying the properties of the flares and compare them with those of the quiescent states. For these sources, the flaring and quiescent states can be clearly defined. Detailed flux variations during a flare and related spectral changes have been obtained. In this paper, we report the results from the studies. In Section 1.1, we describe our target selection. We present the data analysis and results in Section 2 and 3 respectively, and discuss the results in Section 4.

1.1 Target Selection

Using the *Fermi* LAT data, we obtained 90-day binned light curves (9.5 years long) for more than 1800 identified and candidate blazars (Acero et al. 2015) for our systematic study of blazar variability. The choice of 90-day per bin was more for the consideration of computational time required but without losing sensitivity to large flares. For the data selection and analysis, see below Section 2. We went over all the light curves and found nearly 30 loner flare sources. Among them, several events were not blazar flares, but instead were caused by solar flares

or γ -ray bursts occurring in the field (with references to γ -ray solar flare observations¹ and *Fermi*-LAT GRB List of detections²). We excluded those sources, and in the end found 24 blazars with a loner flare. The blazars are listed in Table 1. Most of the flares of the blazars are 10σ – 19σ above the quiescent light curves, while in the cases of J0055.1–1219, J0303.4–2407, J1040.5+0617, and J2134.2–0154, the significances compared to the quiescent light curves are 6.0σ , 7.7σ , 7.1σ , and 9.3σ , respectively.

The class type and redshift information for the blazars are from Chen (2018; see also Acero et al. 2015) and three of them do not have redshifts. In Figure 1, we show their photon indices and luminosities in the quiescent states (three sources without redshifts are not included). Comparing to the whole *Fermi* blazars (cf. Figure 14 in Ackermann et al. 2015), our targets are in a slightly-brighter range, since their luminosities are $\sim 10^{46}$ – 10^{48} ergs⁻¹, except one at $\sim 10^{43}$ ergs⁻¹. The 90-day binned light curves are shown in Figure 2. As can be seen, 20 of them have only one single data point indicating a flare, and the other four have two or three data points in a flare. We note that 20 of them were reported in the second catalog of flaring γ -ray sources (Abdollahi et al. 2017). Previously, the flare of J1153.4+4931 (4C +49.22) was studied with multi-wavelength observations from radio to γ -ray (Cutini et al. 2014), and J0303.4–2407 was reported to have a possible 2.1 yr quasi-periodic modulation in its γ -ray emission (Zhang et al. 2017).

2 Data analysis

2.1 Initial long-term light curve analysis of *Fermi* LAT data

LAT scans the whole sky every three hours in the energy range from 20 MeV to 300 GeV (Atwood et al. 2009). We selected 0.1–300 GeV LAT data from the *Fermi* Pass 8 database. For each of (candidate) blazars, a $20^\circ \times 20^\circ$ square region of interest (ROI) was used, centered at the position of the blazar given in 3FGL (Acero et al. 2015). The time period of the LAT data is 9.5 years from 2008-08-04 15:43:36 (UTC) to 2018-02-08 23:52:17 (UTC). Following the recommendations of the LAT team³, we selected events with zenith angles less than 90 deg to avoid possible contamination from the Earth’s limb.

We constructed light curves binned in 90 day intervals by performing standard binned maximum likelihood analysis. The LAT science tools software package v10r0p5 was used.

¹ http://hesperia.gsfc.nasa.gov/fermi_solar/

² www.asdc.asi.it/grblat/

³ <http://fermi.gsfc.nasa.gov/ssc/data/analysis/scitools/>

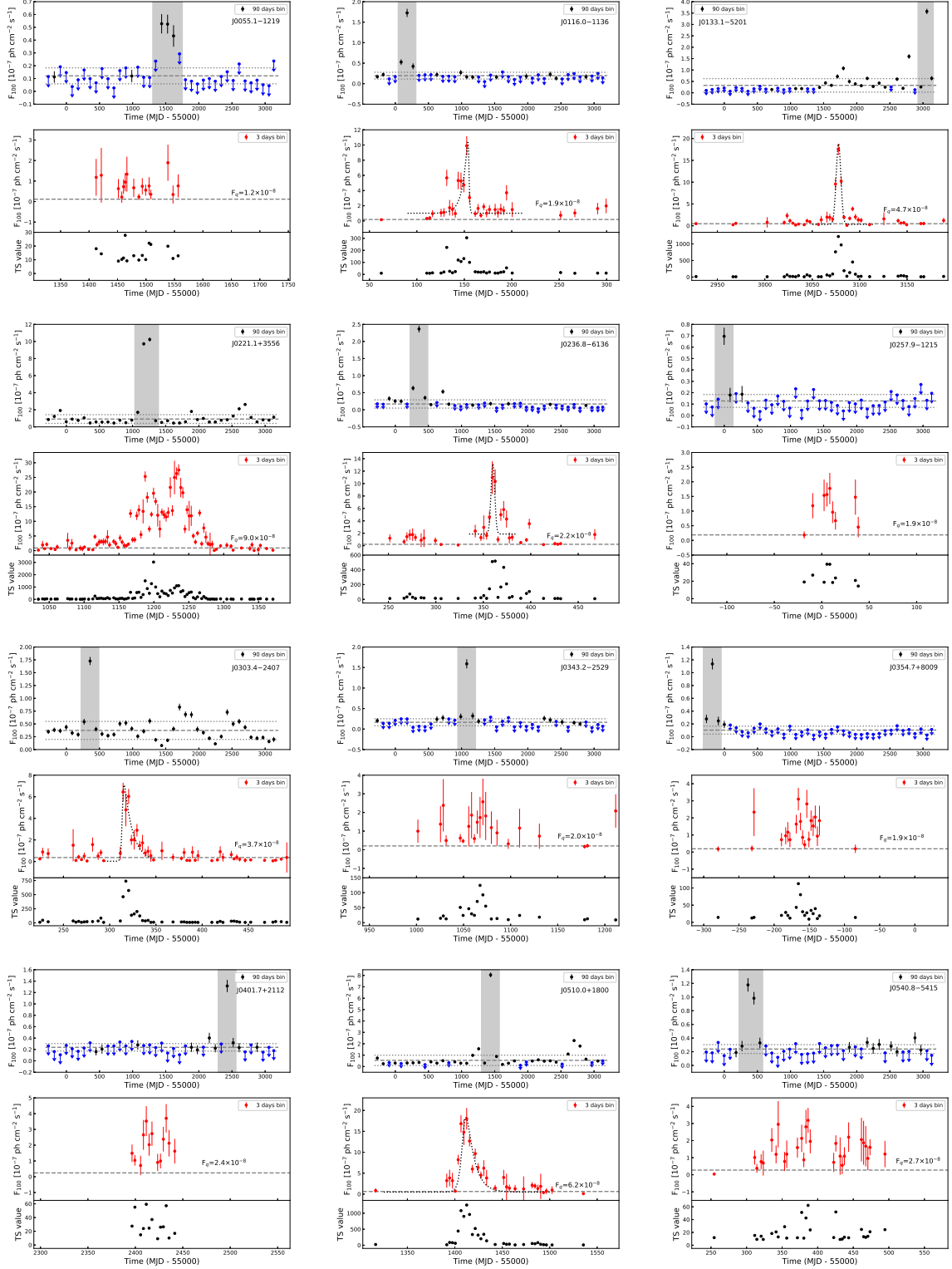


Fig. 2. *Top panels:* light curves binned in 90 day intervals. The average and 1σ range of the quiescent data points are indicated by dashed and dotted lines, respectively. *Bottom panels:* light curves binned in 3 day intervals, the time ranges of which are given by the gray areas in the top panels. When there is a sharp-peak profile contained in a flare, an analytic function (dotted curve) was used to fit the profile. The flux levels of the quiescent states are indicated by dashed lines, with the flux values (F_q) provided.

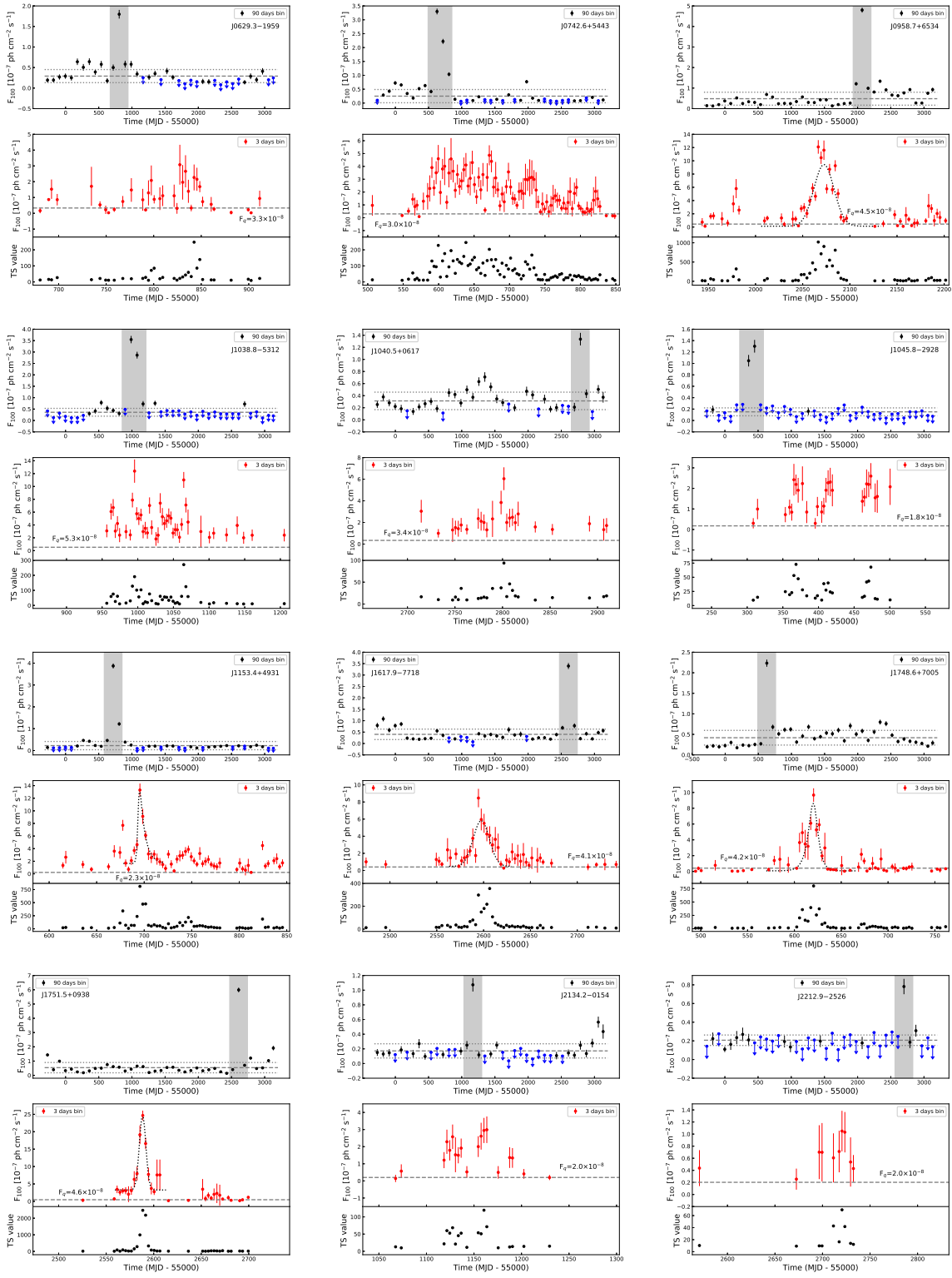


Fig. 2. Continued.

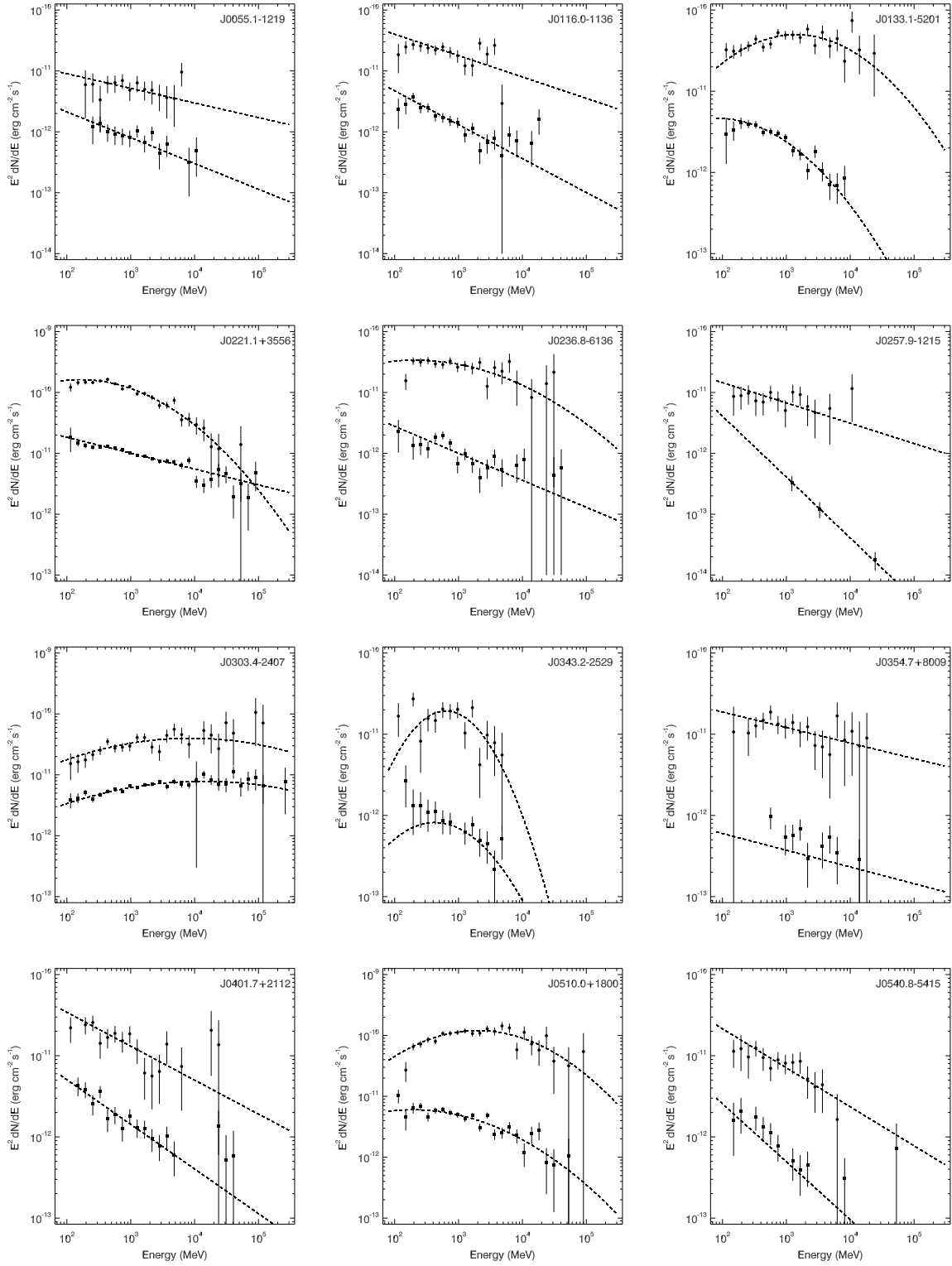


Fig. 3. Spectra of the 24 blazar targets in the flaring (dots) and quiescent (squares) states. The models of either a power law or a log-parabola from the likelihood analysis are shown as dashed lines.

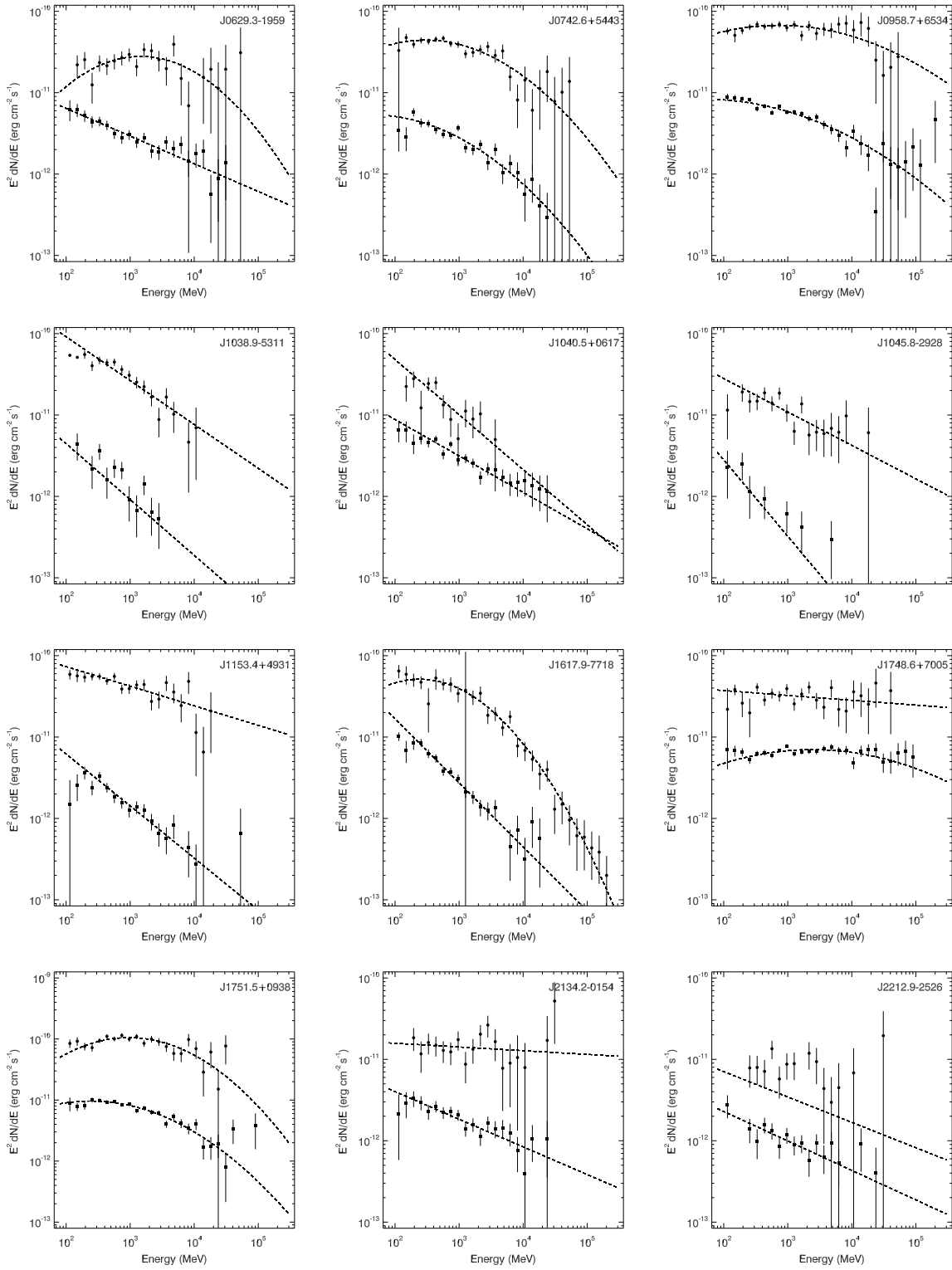


Fig. 3. Continued.

The source model for each blazar was based on 3FGL, and the normalization parameters and spectral indices of the sources within 5 deg from the target as well as sources within the ROI with variable index ≥ 72.44 (Acero et al. 2015) were set as free parameters. All other parameters were fixed at their catalog values in 3FGL. We used the original spectral models in 3FGL for the blazars. Galactic and extragalactic diffuse emission models used were `gllLiem_v06.fits` and `iso_P8R2_SOURCE_V6_v06.txt`, respectively. The normalization parameters of the two diffuse emission components were set as free parameters.

Long-term 90-day binned light curves of more than 1800 (candidate) blazars were obtained. We went over them and determined 24 blazars with a loner flare. Their light curves are shown in the top panels of Figure 2, in which when flux data points have the Test Statistic (TS) values smaller than 9, we calculated their flux upper limits at a 95% confidence level and plotted the upper limits in the light curves.

In order to study detailed flux variations during each flare, we chose a time period around each flare based on the 90-day binned light curves. The region of the time period of a source is indicated by the gray area in Figure 2. Excluding the flare data points in each gray region, those far above the quiescent flux levels (mostly one or two data points), we calculated the average flux and standard deviation of each quiescent light curve. As shown in Figure 2, the flare data points are outstanding, most of which are at least 10σ above the quiescent light curves. We cautiously note that for several cases, there appear to be minor activities, such as in J0133.1–5201, J0303.4–2407, and J1040.5+0617. However for these activities, only a few data points are slightly above the 1σ ranges of the light curves. We thus still considered them as in the quiescent states.

2.2 Detailed Likelihood analysis

Because of the recently released 4FGL, and updated database (P8R3) and background files, we performed detailed likelihood analysis based on them to the LAT data for the 24 selected targets. The same source models were built but based on 4FGL, with Galactic and extragalactic diffuse emission models being `gllLiem_v07.fits` and `iso_P8R3_SOURCE_V2.txt`, respectively.

For the 24 targets, 12 have emission that was described with a simple power law ($dN/dE \propto E^{-\Gamma}$, where Γ is the photon index), and 12 have emission described with a log-parabola ($dN/dE \propto (E/E_0)^{-\alpha-\beta\log(E/E_0)}$, where α and β are spectral parameters. Note that for the latter model when β is small, it is close to being a power law.

We determined the spectral parameters in the quiescent state and for the flare data

points from the likelihood analysis. The values of the spectral parameters Γ_h (or α_h and β_h) in the flaring states and Γ_l (or α_l and β_l) in the quiescent states are given in Table 1.

However from the γ -ray spectra we obtained (see below Section 2.4), we noted that five sources (J0221.1+3556, J0236.8–6136, J0629.3–1959, J1617.9–7718, and J1748.6+7005), provided with spectral models of a log-parabola in 4FGL, might have power-law emission instead, particularly in the quiescent states. We re-ran the likelihood analysis assuming a power-law model for them in the source models, and found that a log-parabola is not significantly preferred over a power law in the quiescent states of the first four sources, while for J1748.6+7005, its emission in the flaring state can be described with a power law. These comparisons were conducted by calculating $\sqrt{-2\log(L_{pl}/L_{logP})}$, where L_{pl} and L_{logP} are the maximum likelihood values obtained from a power law and a log-parabola respectively (Abdo et al. 2013). Therefore in Table 1, we changed these sources' spectral parameters accordingly.

2.3 Fine light curves in flares

For each time period around a flare we chose above, a fine light curve binned in 3-day intervals was constructed, with the middle time of the light curve corresponding to the middle time of the 90-day binned data points of a flare. The choice of 3 days was based on tests of different time intervals, which could well show the details of a flare without having too many flux upper limits in a light curve. For the data in each time bin, the same maximum likelihood analysis as the above was performed. Both light curves and TS curves are shown in the bottom panels of Figure 2. Only the flux data points with $TS > 9$ were kept in the 3-day binned light curves. Comparing to the average quiescent fluxes (F_q given in Figure 2), the light curves show that their high-flux data points in a flare are several tens of times brighter.

2.4 Spectral analysis

We obtained γ -ray spectra for each target in its flaring and quiescent states. The energy range of 0.1 to 300 GeV was evenly divided logarithmically into 30 energy bands. The time ranges of the flaring high-flux data points in the 90-day binned light curves were taken as the flare time durations. In most cases, there is only one data point, implying a 90-day time duration. Excluding the flare data points in each light curves, the other data of a target were analyzed as in the quiescent state. In this analysis, the normalization parameters of all the sources within an ROI and the two diffuse emission components were set as free parameters. The obtained spectra are shown in Figure 3, in which only the spectral data points with $TS > 4$ were kept.

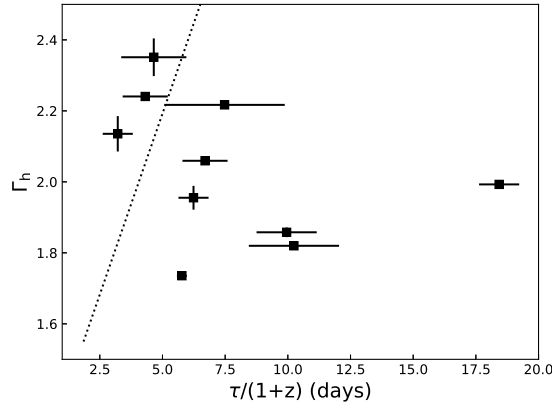


Fig. 4. Time durations of the sharp-peak flares at the local host galaxies. The flares studied in Nalewajko (2013) are above the dotted line, showing that most of our flares have longer time durations.

As shown by the 3-day binned light curves (bottom panels of Figure 2), the detailed flaring activities of a target often spread over part of the region that is not exactly around the center, which is because of our coarse choice of 90-day time intervals. The spectra in the flaring states thus may not be as accurate as possible. However, because the flares are dominantly bright, the results are not significantly affected. We tested to perform likelihood analysis to part of data containing the highest flux data points in the 3-day binned light curves, the obtained spectral results were nearly the same as those obtained from the flare data points.

3 Results

While in 90-day binned light curves, the flares stand out above the low-flux levels of the quiescent states, our detailed light curve analysis shows that only 10 of them contain a sharp peak and the other 14 generally do not have a clear profile. We determined the properties of the 10 sharp-peak cases by fitting their profiles with both a Gaussian function and an analytic function given in Abdo et al. (2010). The former is given by

$$F(t) = F_c + F_0 e^{-(t-t_0)^2/2\sigma_t^2} \quad , \quad (1)$$

where F_c and F_0 are the constant flux and height of a peak, respectively, t_0 is the flux peak time, and σ_t is the standard deviation for measuring the peak time duration. The latter can have an asymmetric profile, given by

$$F(t) = F_c + F_0 (e^{(t_0-t)/T_r} + e^{(t-t_0)/T_d})^{-1} \quad , \quad (2)$$

where T_r and T_d are used to measure the rise and decay time separately. The fitting results are given in Table 2. We chose the better ones based on the reduced χ^2 values, which are

overplotted in the bottom panel of Figure 2. Although the fits seem poor (based on the χ^2 values) and can not describe fine structures of the flares, they allowed us to estimate the time duration of a flare, which is the parameter commonly obtained for blazar flares. The time durations τ of these peaks, defined as when the flux is half of the peak value, were calculated. They are in a range of approximately 4–25 days. In Figure 4, the time durations at the host galaxies ($\tau/(1+z)$) are shown. In addition, comparing F_c and F_0 values with those of the quiescent states, the sharp peaks appear to have contributed primarily to the flaring events.

In 4FGL, our 24 sources have emission half described with a power law and half with a log-parabola. Our detailed analysis shows that in the quiescent states, four of the log-parabola sources are actually well described with a power law, and J1748.6+7005 in the flaring state had emission consistent with being a power law. We note that the spectrum of the last source in the quiescent state also appears flat, although the likelihood analysis indicates that the spectrum is better described with a log-parabola. In any case, we have found four clear cases showing spectral form changes, from a power law in the quiescent state to a log-parabola in the flaring state, which are supported by the their spectra (Figure 3) we obtained. This result is slightly different from previous studies such as in Harris et al. (2014) and Kohler & Nalewajko (2015), since they have found that nearly all the sources kept the same form of emission during flares.

As indicated by both Figure 3 and Table 1, most sources (16 of them) had harder emission when in flares, which is a pattern often seen in bright γ -ray emission of blazars (e.g., Nalewajko 2013; Hayashida et al. 2015; Britto et al. 2016). For the other 8 sources, five did not have significant spectral changes but three of them (J0221.1+3556, J1040.5+0617, and J1748.6+7005) had softer emission when in flares. Examining them, the 3-day binned light curve of J0221.1+3556 shows a complex flaring pattern with two major peaks, while the latter two had relatively “active” quiescent states: J1040.5+0617 had as large as a factor of 3 flux variations and J1748.6+7005 showed minor activities following the flare, and returned to the lowest-flux level at the end of its long-term light curve. These features are noted when comparing them to other sources.

It has been pointed out that since long integration times have to be used in γ -ray observations, in order to collect statistically sufficient photons for analysis, spectra of blazars obtained in most cases are the results of variable emission added together (Kohler & Nalewajko 2015). In our cases, the spectra of the sources in quiescence might particularly have this problem because their spectra were obtained from long-term integrations. We therefore chose three relatively bright sources: J0221.1+3556, J0510.0+1800, and J0958.7+6534, as they were detected in nearly all the 90-day bins. We checked their spectral properties in one year time

durations before and after the flares respectively. The results during the two time periods are consistent within uncertainties; the sources did not have any significant changes in spectra. We thus conclude that the sources likely have relatively stable emission in quiescence before and after the flare.

4 Discussion

Analyzing the 9.5 year γ -ray light curves obtained for the *Fermi* blazars and candidates, we have selected a sample of 24 sources from more than 1800 of them on the basis of the detection of a clear high-flux flaring event in the long-term light curves. The sample differs from other blazars as in most time they have been in a quiescent state with relatively stable emission. We obtained detailed light curves for the flares, and found that 10 of them contain a sharp peak. The time durations of the flares were determined to be in a range of 4–25 days. For most of the other sources, the flares were revealed to be due to random high-flux activity or consist of multiple minor flares, which can not be described by a simple function of time.

In the scenario of having many turbulent cells, multiple subpulses/flares can be naturally produced. Different sizes of emission regions/cells or different magnetization parameters ($\sigma = P_B/P_k$, where P_B and P_k are the magnetic and kinetic power, respectively) can result in various spike patterns on the overall light curve (Zhang & Zhang 2014). This turbulent process may thus be the reason for the generally two types of profiles in the flares of our sample. Multiple minor flares could be due to enhanced emission from multiple turbulent cells, and a sharp-peak flare would arise from a single dominant turbulent cell. We note that the sharp-peak events have relatively long time durations. For example, in Figure 4, a dotted line marks the approximate low boundary of the bright flares studied in Nalewajko (2013). Note that the time durations of these flares were defined as the flux doubling time plus the flux halving time, but in any case only three of our sharp-peak flares are in the region (Figure 4). The other seven are not, with the time durations at the host galaxies in a range of 5–19 days. In addition, the emission in these seven cases tended to be hard, five of them having Γ_h (or α_h) smaller than 2.0, among the lowest in our sample (see Figure 5). We thus suspect that these hard-emission, sharp peak flares may provide additional insight into the physical properties of a single turbulent cell.

More than half of our sample sources showed harder emission during the flares, while five of them did not have any significant changes and three of them had softer emission in their flares. We searched through possible correlations between fluxes/luminosities and photon indices during the flaring and quiescent states, where for log-parabola cases we used α_h or

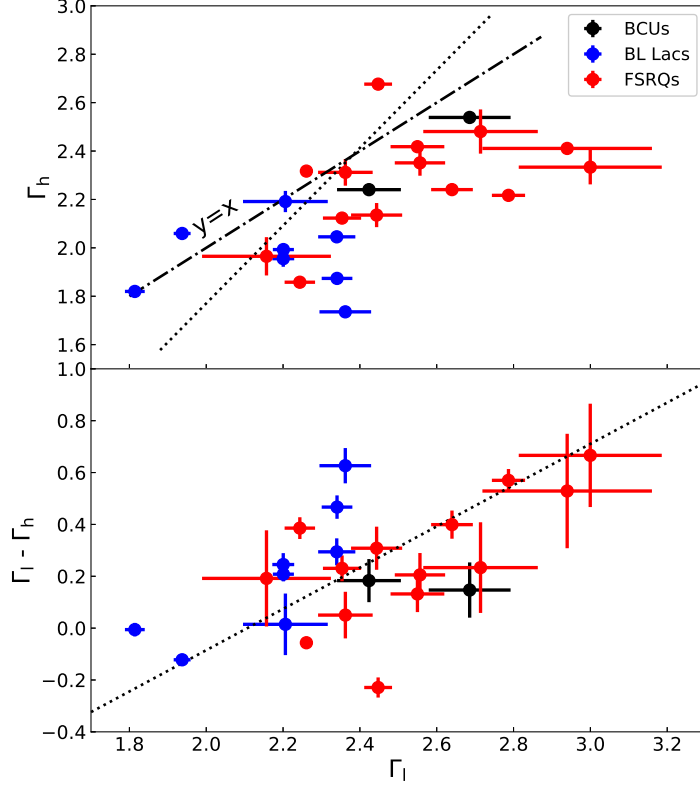


Fig. 5. *Top panel:* photon indices of 24 blazars in the quiescent (Γ_l or α_l) and flaring (Γ_h or α_h) states. A possible correlation of $\Gamma_h \sim 1.6\Gamma_l$ is indicated by a dotted line in the top panel. For a comparison, a $\Gamma_h = \Gamma_l$ line (long-dash dotted line) is also shown. *Bottom panel:* $\Gamma_l - \Gamma_h$ versus Γ_l , with a possible relationship shown as a dotted line.

α_l as the indices since they define the slope of a spectrum. Nothing significant was found except a possible correlation between Γ_h and Γ_l : $\Gamma_h \sim 1.6\Gamma_l$ (see the top panel of Figure 5), The Pearson correlation coefficient is 0.62. However it is hard to derive obvious physical connections between them, as why the enhanced emission during flares would be in some way connected to quiescent emission. If we plot $\Gamma_l - \Gamma_h$ versus Γ_l instead (the bottom panel of Figure 5), a trend of $(\Gamma_l - \Gamma_h) \sim 0.8\Gamma_l$ is seen, although with a couple of data points significantly deviating away from the trend. The trend may be understood as that the larger Γ_l , the larger the changes. In other words, as most blazars turn to be harder when they are brighter in flares, and if Γ_h are in a certain range, sources with larger deviations from the range during quiescence would have larger changes to jump back during flares. Further investigation on this possible property can be conducted with studying a large sample of flares with clear quiescent levels.

In our cases, the spectra of FSRQs in either the flares or quiescence do not show any clear breaks (or cutoffs) at the GeV energy band, and half of them show spectra that extend beyond ~ 20 GeV. The presence of significant spectral breaks at GeV energies in several blazars

has been suggested due to the absorption by photons from the broad line region (BLR) through the pair production process (Finke & Dermer 2010; Poutanen & Stern 2010), while later large-sample studies have indicated that the absorption is not universal and most blazars do not present the spectral feature (e.g., Costamante et al. 2018; Meyer et al. 2019). Therefore, the γ -ray emission regions of our blazar sources are expected to lie beyond the BLR (Liu & Bai 2006), which are consistent with SED modeling of a large sample of blazars (Kang et al. 2014). The emission regions may still be within the dust torus, and relativistic electrons in a jet will inverse Compton (IC) scatter the infrared (IR) photons from the dust torus, producing the observed γ -rays. As a result, the electrons will be cooled with time scale $T_{cooling} \approx 2.5 \times 10^7 (\nu_{ext}/\nu_{IC})^{1/2} \Gamma_j^{-3/2} \delta_j^{-1/2} U_{ext}^{-1}$ s, where $\nu_{ext} \sim 3 \times 10^{13}$ Hz and $U_{ext} \sim 3 \times 10^{-4}$ erg cm $^{-3}$ are the peak frequency and energy density of the torus IR radiation. Applying the typical values for the bulk Lorentz factor Γ_j and Doppler beaming factor δ_j of a blazar jet, $\Gamma \approx \delta \approx 10$, $T_{cooling} \sim 0.1$ days for ~ 1 GeV γ -rays ($\nu_{IC} = 1$ GeV = 2.4×10^{23} Hz). The cooling time is much smaller than the observed time durations of the sharp-peak flares (4–25 days), indicating that the energetic electrons in these jet cases may be in-situ accelerated.

As a summary, our studies of these 24 loner flares have revealed the different variation profiles in their detailed light curves and the spectral property of having harder emission in flares in most cases. Different from those obtained in bright flares, clear spectral form changes were seen in four cases. We have also found a possible trend between $\Gamma_l - \Gamma_h$ and Γ_l and a tendency of having long flaring time durations and hard emission in the sharp-peak flare cases. However, our sample is small, and no firm conclusions can be drawn for these two possible features. For the purpose of enlarging our sample, similar studies can be carried out by including those sources with multiple flares in their long-term light curves. Given 1000 more blazars are preliminarily listed in the fourth *Fermi* LAT AGN catalog (The Fermi-LAT collaboration 2019b), similar work can also be extended to the new sources. Thus statistically significant relations may be established, helping our understanding of blazar flares and related physical processes.

This research made use of the High Performance Computing Resource in the Core Facility for Advanced Research Computing at Shanghai Astronomical Observatory. This research was supported by the National Program on Key Research and Development Project (Grant No. 2016YFA0400804) and the National Natural Science Foundation of China (11633007, U1738131).

References

- Abdo, A. A., Ackermann, M., Ajello, M., et al. 2010, *ApJ*, 722, 520
- Abdo, A. A., Ajello, M., Allafort, A., et al. 2013, *ApJS*, 208, 17
- Abdollahi, S., Ackermann, M., Ajello, M., et al. 2017, *ApJ*, 846, 34
- Acero, F., Ackermann, M., Ajello, M., et al. 2015, *ApJS*, 218, 23
- Ackermann, M., et al. 2015, *Astrophys. J.*, 810, 14
- Ackermann, M., Anantua, R., Asano, K., et al. 2016, *ApJL*, 824, L20
- Atwood, W. B., Abdo, A. A., Ackermann, M., et al. 2009, *ApJ*, 697, 1071
- Britto, R. J., Bottacini, E., Lott, B., Razzaque, S., & Buson, S. 2016, *ApJ*, 830, 162
- Chatterjee, R., Jorstad, S. G., Marscher, A. P., et al. 2008, *ApJ*, 689, 79
- Chatterjee, R., Bailyn, C. D., Bonning, E. W., et al. 2012, *ApJ*, 749, 191
- Chen, L. 2018, *ApJS*, 235, 39
- Costamante, L., Cutini, S., Tosti, G., Antolini, E., & Tramacere, A. 2018, *MNRAS*, 477, 4749
- Cutini, S., Ciprini, S., Orienti, M., et al. 2014, *MNRAS*, 445, 4316
- Dermer, C. D., & Giebels, B. 2016, *Comptes Rendus Physique*, 17, 594
- Finke, J. D., & Dermer, C. D. 2010, *ApJL*, 714, L303
- Harris, J., Chadwick, P. M., & Daniel, M. K. 2014, *MNRAS*, 441, 3591
- Hayashida, M., Nalewajko, K., Madejski, G. M., et al. 2015, *ApJ*, 807, 79
- Kang, S.-J., Chen, L., & Wu, Q. 2014, *ApJS*, 215, 5
- Kohler, S., & Nalewajko, K. 2015, *MNRAS*, 449, 2901
- Kushwaha, P., Singh, K. P., & Sahayanathan, S. 2014, *ApJ*, 796, 61
- Liu, H. T., & Bai, J. M. 2006, *ApJ*, 653, 1089
- Madejski, G. ., & Sikora, M. 2016, *ARA&A*, 54, 725
- Meyer, M., Scargle, J. D., & Blandford, R. D. 2019, *ApJ*, 877, 39
- Nalewajko, K. 2013, *MNRAS*, 430, 1324
- Poutanen, J., & Stern, B. 2010, *ApJL*, 717, L118
- The Fermi-LAT collaboration. 2019a, arXiv e-prints, arXiv:1902.10045
- . 2019b, arXiv e-prints, arXiv:1905.10771
- Ulrich, M.-H., Maraschi, L., & Urry, C. M. 1997, *ARA&A*, 35, 445
- Zhang, B., & Zhang, B. 2014, *ApJ*, 782, 92
- Zhang, P.-F., Yan, D.-H., Zhou, J.-N., et al. 2017, *ApJ*, 845, 82

Table 1. 24 blazar sources and their spectral properties

Source name	Class	z	Association	Spectral model	$\Gamma_h (\alpha_h)$	β_h	$\Gamma_l (\alpha_l)$	β_l	$\Delta\Gamma$
J0055.1–1219	BCU	-	TXS 0052–125	PowerLaw	2.24 ± 0.002		2.42 ± 0.08		0.18 ± 0.08
J0116.0–1136	CF	0.670	PKS 0113–118	PowerLaw	2.35 ± 0.05		2.56 ± 0.07		0.21 ± 0.08
J0133.1–5201	UB	0.020	PKS 0131–522	LogParabola	1.74 ± 0.01	0.11 ± 0.004	2.36 ± 0.07	0.11 ± 0.03	0.63 ± 0.07
J0221.1+3556*	CF	0.685	S3 0218+35	LogParabola	2.32 ± 0.01	0.10 ± 0.004	2.26 ± 0.02		-0.06 ± 0.02
J0236.8–6136*	CF	0.465	PKS 0235–618	LogParabola	2.14 ± 0.05	0.06 ± 0.03	2.44 ± 0.07		0.31 ± 0.08
J0257.9–1215	CF	1.391	PMN J0257–1211	PowerLaw	2.33 ± 0.07		3.00 ± 0.19		0.67 ± 0.20
J0303.4–2407	CB	0.260	PKS 0301–243	LogParabola	1.82 ± 0.002	0.04 ± 0.001	1.81 ± 0.03	0.03 ± 0.01	-0.006 ± 0.03
J0343.2–2529	CF	1.419	PKS 0341–256	LogParabola	1.97 ± 0.08	0.39 ± 0.06	2.16 ± 0.17	0.22 ± 0.09	0.19 ± 0.19
J0354.7+8009	CB	-	S5 0346+80	PowerLaw	2.19 ± 0.04		2.21 ± 0.11		0.01 ± 0.12
J0401.7+2112	CF	0.834	TXS 0358+210	PowerLaw	2.42 ± 0.001		2.55 ± 0.07		0.13 ± 0.07
J0510.0+1800	CF	0.416	PKS 0507+17	LogParabola	1.86 ± 0.01	0.11 ± 0.01	2.24 ± 0.04	0.07 ± 0.02	0.39 ± 0.04
J0540.8–5415	CF	1.185	PKS 0539–543	PowerLaw	2.48 ± 0.09		2.71 ± 0.15		0.23 ± 0.17
J0629.3–1959*	CB	1.724	PKS 0627–199	LogParabola	1.87 ± 0.02	0.12 ± 0.01	2.34 ± 0.04		0.47 ± 0.05
J0742.6+5443	CF	0.720	GB6 J0742+5444	LogParabola	2.12 ± 0.001	0.08 ± 0.001	2.35 ± 0.05	0.07 ± 0.03	0.23 ± 0.05
J0958.7+6534	CB	0.368	S4 0954+65	LogParabola	1.99 ± 0.004	0.04 ± 0.002	2.20 ± 0.03	0.04 ± 0.01	0.21 ± 0.03
J1038.8–5312	BCU	-	MRC 1036–529	PowerLaw	2.54 ± 0.001		2.69 ± 0.11		0.15 ± 0.11
J1040.5+0617	UF	2.715	GB6 J1040+0617	PowerLaw	2.68 ± 0.01		2.45 ± 0.04		-0.23 ± 0.04
J1045.8–2928	CF	2.128	PKS B1043–291	PowerLaw	2.41 ± 0.001		2.94 ± 0.22		0.53 ± 0.22
J1153.4+4931	CF	0.925	4C +49.22	PowerLaw	2.24 ± 0.002		2.64 ± 0.05		0.40 ± 0.05
J1617.9–7718*	CF	1.710	PKS 1610–77	LogParabola	2.22 ± 0.01	0.13 ± 0.004	2.79 ± 0.04		0.57 ± 0.04
J1748.6+7005*	CB	0.770	S4 1749+70	LogParabola	2.06 ± 0.002		1.94 ± 0.02	0.04 ± 0.01	-0.12 ± 0.02
J1751.5+0938	CB	0.322	OT 081	LogParabola	1.96 ± 0.03	0.12 ± 0.02	2.20 ± 0.03	0.08 ± 0.02	0.25 ± 0.04
J2134.2–0154	CB	1.283	PKS 2131–021	PowerLaw	2.05 ± 0.02		2.34 ± 0.05		0.29 ± 0.05
J2212.9–2526	CF	1.833	PKS 2210–25	PowerLaw	2.31 ± 0.06		2.36 ± 0.07		0.05 ± 0.09

Notes: Class and redshift information for the sources are from Chen (2018), where “UF” are blazar candidates of uncertain type (BCUs) classified as FSRQs, “UB” the BCUs classified as BL Lacs, and “CF” and “CB” are confirmed FSRQs and BL Lacs, respectively. *: sources without β_h or β_l are described with a power law instead.

Table 2. Fitting results for the flaring peaks in 10 sources

Source name	F_c ($\times 10^{-7}$)	F_0 ($\times 10^{-7}$)	t_0 (MJD)	σ_t (day)	T_r (day)	T_d (day)	χ^2/dof
J0116.0–1136	0.8 ± 0.1	6.1 ± 0.8	55151.2 ± 0.9	4.8 ± 0.6			76.1/22
	1.0 ± 0.1	12.7 ± 2.5	55154.8 ± 0.9		5.4 ± 1.1	0.5 ± 0.2	64.0/21
J0133.2–5201	0.3 ± 0.1	18.5 ± 1.3	58077.7 ± 0.5	2.5 ± 0.1			96.0/12
	0.1 ± 0.1	24.0 ± 2.3	58080.0 ± 0.7		4.1 ± 0.4	1.3 ± 0.2	121.8/11
J0236.8–6136	1.9 ± 0.3	11.3 ± 2.7	55360.1 ± 1.3	2.0 ± 0.3			32.8/9
	2.0 ± 0.4	13.1 ± 6.7	55361.6 ± 1.9		3.0 ± 1.3	0.8 ± 0.7	39.5/8
J0303.4–2407	0.5 ± 0.1	4.8 ± 0.8	55319.1 ± 1.5	4.7 ± 0.6			60.9/9
	0.0 ± 0.2	9.5 ± 1.8	55313.8 ± 1.6		0.8 ± 0.3	9.0 ± 1.5	21.5/8
J0510.0+1800	1.4 ± 0.1	16.7 ± 1.7	56412.7 ± 1.2	4.7 ± 0.3			170.0/23
	0.5 ± 0.1	31.0 ± 4.7	56409.5 ± 1.3		2.6 ± 0.2	8.1 ± 1.0	95.6/22
J0958.7+6534	0.1 ± 0.1	9.3 ± 0.5	57072.5 ± 0.7	10.7 ± 0.4			135.9/21
	0.0 ± 0.1	18.6 ± 2.1	57066.6 ± 1.6		5.7 ± 0.4	12.2 ± 1.8	149.6/20
J1153.4+4931	1.8 ± 0.3	10.6 ± 1.2	55696.8 ± 1.1	3.4 ± 0.3			23.6/10
	1.6 ± 0.3	17.5 ± 2.2	55693.8 ± 1.1		0.9 ± 0.2	5.4 ± 0.7	16.9/9
J1617.9–7718	0.5 ± 0.3	5.3 ± 0.7	57597.5 ± 1.0	8.6 ± 1.2			34.8/17
	0.3 ± 0.3	11.8 ± 1.8	57597.9 ± 1.5		6.9 ± 1.4	6.6 ± 1.6	34.3/16
J1748.6+7005	0.1 ± 0.0	7.8 ± 0.6	55620.4 ± 0.2	8.8 ± 0.3			43.4/18
	0.1 ± 0.0	16.9 ± 1.3	55620.7 ± 0.3		5.0 ± 0.5	4.0 ± 0.4	40.2/17
J1751.5+0938	3.3 ± 0.4	21.3 ± 4.6	57588.3 ± 4.1	3.5 ± 0.3			4.3/12
	3.4 ± 0.4	54.4 ± 16.4	57589.4 ± 5.8		2.2 ± 0.4	2.1 ± 0.2	28.0/11

Notes: F_c and F_0 are in units of $\text{ph cm}^{-2} \text{s}^{-1}$. χ^2/dof are χ^2 value and degrees of freedom for the fitting to the sharp-peak flares.